

This work was written as part of one of the author's official duties as an Employee of the United States Government and is therefore a work of the United States Government. In accordance with 17 U.S.C. 105, no copyright protection is available for such works under U.S. Law.

Public Domain Mark 1.0

<https://creativecommons.org/publicdomain/mark/1.0/>

Access to this work was provided by the University of Maryland, Baltimore County (UMBC) ScholarWorks@UMBC digital repository on the Maryland Shared Open Access (MD-SOAR) platform.

Please provide feedback

Please support the ScholarWorks@UMBC repository by emailing scholarworks-group@umbc.edu and telling us what having access to this work means to you and why it's important to you. Thank you.



Contents lists available at ScienceDirect

Journal of Quantitative Spectroscopy and Radiative Transfer

journal homepage: www.elsevier.com/locate/jqsrt

Evaluation of EPIC oxygen bands stability with radiative transfer simulations over the South Pole

Yaping Zhou^{a,b,*}, Peng-Wang Zhai^c, Yuekui Yang^a

^a NASA Goddard Space Flight Center, Greenbelt, MD, United States

^b GESTAR II/University of Maryland Baltimore County, Baltimore, MD, United States

^c GESTAR II/Department of Physics, University of Maryland Baltimore County, Baltimore, MD 21250, United States

ARTICLE INFO

Keywords:

EPIC
DSCOVR
Radiative transfer model simulation
South Pole
Calibration
Remote sensing

ABSTRACT

The Earth Polychromatic Imaging Camera (EPIC) onboard the Deep Space Climate Observatory (DSCOVR) satellite orbiting the Sun at the Lagrange-1 point was launched without onboard calibration systems. Vicarious calibration is conducted for 8 of the 10 UV/VIS/NIR channels using other low earth orbiting satellite instruments, while its two O₂ bands (688 nm and 764 nm) rely on indirect moon-view calibrations because the same narrow-band O₂ bands are not readily available from other in-flight instruments. This study compares EPIC measurements from the four O₂ bands aiming at examining sensor stability over a uniquely suited location, i.e., the permanently snow-covered South Pole. The study utilizes radiative transfer model simulations with in-situ atmospheric soundings taken at South Pole during months of December and January from 2015 to 2022. The absolute discrepancy between the model simulations and observations is less than 1.0% for the two reference bands, but 5.75% and 15.63% for the 688 nm, and 764 nm absorption bands, respectively. The simulated A-band and B-band ratios are 16.09% and 4.74% higher than that from the observations. Various sensitivities are conducted to estimate possible contributions to the discrepancies from input atmospheric profiles, spectral surface albedos and surface BRDF. While none of the input uncertainties is likely to account for the large discrepancies in the oxygen absorption bands, a small shift in the instrument response function could be the main reason for these biases. On the other hand, the model simulations are able to capture systematic variations with observed angular measurements and explain the multi-year trends found in observed O₂ band ratios due to satellite orbit shifting. When model simulated contributions from the angle variations are deducted from the observed O₂ band ratios, the residual O₂ band ratios are found to be stable since 2015.

1. Introduction

The Earth Polychromatic Imaging Camera (EPIC) is a 10-channel spectroradiometer (317 – 780 nm) onboard NOAA's Deep Space Climate Observatory (DSCOVR) satellite orbiting the sun at the Lagrange-1 point, L1, about 1.5 million kilometers away from Earth. EPIC's spectral channels include four (317 nm, 325 nm, 340 nm, 388 nm) in ultraviolet (UV) and six (443 nm, 551 nm, 680 nm, 687.75 nm, 764 nm, 779.5 nm) in visible/near-infrared (Vis/NIR) spectral regions. Among these channels, there are two pairs of O₂ bands with the absorption bands centered at 688 nm (B-band) and 764 nm (A-band) and a nearby non-absorbing reference band at 680 nm and 780 nm,

respectively. The EPIC observations provide retrievals of total column ozone, sulfur dioxide, aerosol, cloud, and vegetation, etc. for the sun-lit side of the Earth every 1~2 hrs [1,2]. The O₂ bands are used extensively in the retrieval of EPIC cloud products [3]. The retrieval of cloud effective pressure and height are essentially based on O₂ band ratios. In addition, the O₂ band ratios are used innovatively in the cloud mask over ice and snow surfaces [4] and ocean glint regions [5]. The O₂ band is also used in the retrieval of smoke and dust plume height [6,7] and cloud screening in aerosol retrieval [8].

Quality retrievals rely on stability of the instrument and good radiometric calibrations. Since EPIC was launched without an accurate laboratory calibration and in-flight calibration devices, in-flight

Submitted to Journal of Quantitative Spectroscopy and Radiative Transfer
Jul 18, 2023

* Corresponding author at: NASA Goddard Space Flight Center, Greenbelt, MD, United States.

E-mail address: yaping.zhou-1@nasa.gov (Y. Zhou).

<https://doi.org/10.1016/j.jqsrt.2023.108737>

Received 7 February 2023; Received in revised form 18 July 2023; Accepted 21 July 2023

Available online 30 July 2023

0022-4073/© 2023 Published by Elsevier Ltd.

calibration using other well-calibrated low earth orbit (LEO) or geostationary orbit (GEO) satellites was necessary. For the UV bands, the LEO instruments Aura/OMI (Ozone Monitoring Instrument) and Suomi-NPP/OMPS (National Polar-orbiting Partnership /Ozone Mapping and Profiler Suite) contain similar wavelengths and are able to observe scenes that closely match in location and angles with those observed by EPIC [9]. For the visible and NIR (443 nm, 551 nm, 680 nm, and 780 nm) calibrations, instruments such as MODIS, MISR and VIIRS can similarly provide well-calibrated measurements [10,11]. However, these instruments do not have the corresponding O₂ absorption bands in 688 nm and 764 nm. Currently, the O₂ band calibration uses lunar observations when the EPIC instrument points to the fully luminated moon surface [10]. The assumption is that the pair of O₂ bands would have similar lunar reflectance (~1.0% difference) because of their small wavelength difference in the absence of any gaseous absorptions and scatterings in their path. The slight difference in the wavelengths in (680 nm and 688 nm) and (780 nm and 764 nm) were considered by assuming that lunar surface reflectance increases approximately 0.8–1.2% with every 10 nm increase in wavelength from previous lunar observations [12], which leads to an assumed reflectance ratio of 1.008 for R₆₈₈/R₆₈₀ and 0.984 for R₇₆₄/R₇₈₀. Thus the O₂ band calibrations rely on the absolute calibration of 680 nm and 780 nm from other GEO/LEO instruments, a ratio of electronic counts at the lunar view from absorption and reference channel, as well as the assumption of fixed lunar reflectance ratio. Each of the three components could contribute some uncertainty to the O₂ band calibrations. Since this calibration is done in the absence of actual O₂ absorption, it is harder to identify detector related changes. Small shift in the instrument response function (IRF) may have little effect on the reflectance in a non-absorptive environment, but due to the nature of O₂ absorption lines it may lead to large difference in the radiative transfer model (RTM) simulations that assume the pre-launch IRF. Subsequently this could lead to errors in retrievals that use RTM generated lookup table (LUT) such as cloud effective height algorithm.

In order to monitor the performance of the O₂ A- and B-band and ensure the absolute calibration of these channels, the EPIC cloud algorithm team has been monitoring the EPIC measurements of these channels over the Amundsen–Scott South Pole Station. We select the South Pole location because of its homogenous bright surface and high elevation. As a result, most of the signal received by the EPIC sensor comes from the surface; hence the photon path length is well defined and the ratio calculations are less prone to noise [13,14]. In addition, the sky conditions at the South Pole station are routinely recorded and radiosondes are launched at least once daily to measure the atmospheric temperature and humidity profiles. Ozonesondes are also launched regularly, albeit less frequently than the radiosonde, to monitor the atmospheric ozone distribution and total amount. These in-situ measurements in combination with a radiative transfer model (RTM) will allow simulation of expected reflectances received by the EPIC instrument.

This study explores the unique South Pole location and RTM simulations to evaluate the stability and calibration of the EPIC instrument. To further minimize meteorological impacts on the measurements, we focus on the EPIC clear sky measurements taken during the austral summer months of December and January each year from 2015 to 2022. To understand the small fluctuations and multi-year trends in the EPIC's O₂ bands and ratios, we performed RTM simulations with inputs from radiosonde profiles and column ozone observation when these measurements are available. Section 2 describes ground and in-situ observational data in the South Pole and RTM model used. Section 3 presents comparison of model simulations with the observed reflectance and sensitivities studies. Section 4 investigates the causes of “trends” observed in the December and January reflectance time series. Section 5 is a summary of the study.

2. Data and methodology

2.1. South Pole observations

The Amundsen-Scott South Pole Station is a year-round US Meteorological/Weather station established in 1957. The station is equipped with many standard meteorological instruments and takes routine measurements of temperature, wind, and pressure from both the surface and the upper levels of the atmosphere. Many additional instruments were placed in South Pole over the time to measure surface radiation, air composition, ozone etc. to support various research projects. The station is located exactly at the south pole (90°S, 2836 m above mean sea level). We obtained the surface sky observations and radiosonde profiles archived at the Antarctic Meteorological Research Center (AMRC) at the University of Wisconsin-Madison [15]. The surface sky observations were taken manually every 3 h indicating cloud fraction in octave scale. Clear sky is identified with a "SKC" classification. The radiosonde profiles consist of measurements of pressure, temperature, dew point, and relative humidity. In addition, we obtained South Pole column total ozone from the Global Monitoring Laboratory of the NOAA Earth System Research Laboratory (ESRL) (<https://gml.noaa.gov/ozwv/ozsondes/spo.html>)

Routine ozone profiles are measured at Amundsen-Scott South Pole Station by balloon-borne electrochemical concentration cell (ECC) ozonesondes, available since 1967 [16]. Total column ozone is calculated by integrating the ozone partial pressure profile up to the balloon burst altitude (around 35 km) and adding a residual amount, based on climatological ozone tables, to account for ozone above the balloon burst altitude. While radiosondes are usually launched twice daily at 00Z and 12Z, the ozonesondes are taken every 5–10 days and data must be interpolated to the days RTM calculations occur.

To monitor the stability of O₂ bands, pixels from EPIC L1B granules corresponding to South Pole were selected from December and January of each year, starting from December 2015. Due to EPIC's L1 orbit, it observes most of the sunlit disk of the Earth including South Pole from nearly backscatter direction. A typical EPIC pixel at South Pole during December to January has a solar zenith angle (SZA) between 67° to 73°, view zenith angle (VZA) between 61° to 74° and backscattering azimuth angle greater than 165° (Fig. 5). The EPIC pixel size increases with VZA as its pixel shape changes from 10 km circle from nadir to an elongated ellipse with its longer axis reaching 20–30 km (approximately 1/cos(VZA)) at 67° to 73° VZA at South Pole. The collocation requires EPIC pixels to be less than 0.25 h and 0.1 deg (~10 km) in latitude from South Pole's surface clear sky measurements (0/8 cloudy). In addition, the pixels must also be clear based on the EPIC cloud mask algorithm [5]. A total of 3978 such pixels are identified. However, to evaluate these measurements with RTM simulations, we further narrow the EPIC measurements to be taken within 0.5 hour of the 1200Z radiosonde measurements to minimize the diurnal variation of reflectance and to ensure that model input profiles best represent the in-situ atmospheric conditions the EPIC instrument was observing.

It must be noted that even with 0.1° distance requirement, multiple EPIC pixels from a same granule will meet the collocation requirements. We use pixels with relative azimuth angles greater than 160° to produce an average reflectance for the time. Pixels with relative azimuth angles smaller than 160° rarely happen and the reflectance could depart more from the rest of pixels hence removed from consideration. The variation of the angles as well as the reflectance among the remaining pixels are small enough that a mean reflectance of these pixels is used to minimize the noise. These processes further reduce the clear sky measurements to 74 instantaneous granules with available radiosonde at 1200Z.

2.2. EPIC simulator

An EPIC simulator [17] has been built upon a radiative transfer model based on the successive order of scattering method (RTSOS) [18,

19] that solves multiple scattering of monochromatic light in the atmosphere and surface systems. RTSOS considers gas absorptions due to ozone, oxygen, water vapor, nitrogen dioxide, methane, and carbon dioxide wherever applicable to EPIC bands. The gas absorption cross sections as a function of atmospheric pressure and temperature are computed from the HITRAN line database [20] using the Atmospheric Radiative Transfer Simulator (ARTS) [21]. In the O₂ A- and B-bands, radiances from line-by-line radiative transfer simulations are computed and then convolved with the EPIC instrument response functions. The EPIC simulator is used to generate the oxygen A-band and B-band reflectance, from which the oxygen band ratios are computed. It has been used as an algorithm developing tool for the EPIC cloud product [4, 5]. The current version of the model has incorporated an improved pseudospherical shell (IPSS) approximation of the earth's surface, for which the solutions to single and multiple scattering are treated separately [22]. The single scattering component is solved exactly for the spherical shell atmosphere. The multiple to single scattering ratio is solved using the plane parallel (PPL) geometry [19]. The IPSS method is an improvement to the so-called pseudo-spherical shell (PSS) approximation, which treats the direct solar beam attenuation along the nadir view in the spherical atmosphere while keeping the PPL geometry for the multiple scattering calculations [23]. The IPSS is important in this study because both the solar and viewing zenith angles are large at the South Pole location.

In our previous studies, we used default model atmosphere, i.e., standard US atmosphere or subarctic summer atmosphere (SSA) from the Intercomparison of Radiation Codes in Climate Models (ICRCCM) project [24], to assess the sensitivities of model reflectance to specific clouds. However, the variation of atmospheric profiles and compositions will affect total amount of molecules (thus Rayleigh scattering) and the amount of dominant absorbing gas O₂ and other trace gases, hence we will input in-situ observation-based profiles as much as possible. The current study requires more accurate atmospheric conditions for clear sky reflectance simulations. We replaced the total molecular number density and the H₂O mixing ratio in the SSA with the in-situ radiosonde measurements from the surface (2.836 km above sea level or around 660 mb) up to the level of radiosonde outburst (around 26 km or 16 mb during the austral summer months). The total molecular number density was computed from pressure and temperature using the ideal gas law at each level (Eq. (2)), while the H₂O molecular number density was converted from mixing ratio, temperature, and pressure (Eq. (4)). The O₂ and CO₂ number densities are proportionally changed with the total molecular density at each level assuming their percentages in number density are fixed. The vertical profiles above the radiosonde records remain unchanged. The ozone density was scaled with observed total column ozone from the ozonsonde. Other trace gases, e.g. nitrogen dioxide and methane are taken from the default SSA profile.

The following equations are used to compute the H₂O and total molecular densities from radiosonde measurements of air temperature, pressure and mixing ratio.

$$PV = nRT \quad (1)$$

$$\rho = n \frac{N_a}{V} = \frac{PN_a}{RT} \quad (2)$$

$$e = \frac{rP}{\left(r + \frac{M_w}{M_d}\right)} \quad (3)$$

$$\rho_{h_2o} = e * \frac{N_a}{RT} \quad (4)$$

In the above, P , T and r are radiosonde measurements of pressure, temperature and mixing ratio respectively; n is number of molecules in mole; V is gas volume; P is the vapor pressure; ρ and ρ_{h_2o} are total and water vapor number density, respectively. M_w , M_d , R and N_a are four constants, representing molar mass of water and dry air, universal gas

constant and the Avogadro number, respectively.

Besides the vertical profiles, the RTM requires input of ground altitude. Surface albedo and bidirectional reflectance distribution function (BRDF) is critical in determining the TOA reflectance. Historic measurements of spectral albedos in Antarctica over snow surface ranges from 0.92 from visible/NIR region to 0.99 in the UV region [25,26]. To facilitate more accurate simulations of TOA reflectance, the current EPIC simulator has enabled spectrally varying albedo input for each channel while previous version only allows a single albedo input for all channels. In addition, we have implemented an empirical snow surface BRDF which is based on in-situ surface BRDF observations at Dome C in Antarctic [26]. The spectral albedo measurements at Dome C from the same paper is chosen as default surface spectral albedo. Since spectral albedo and surface BRDF at high angles could represent a large source of uncertainty, we conducted sensitivities with surface albedo and BRDF to examine possible effect for the simulated reflectances.

Other inputs for the EPIC simulator include specifications of the sun and sensor-view geometry, i.e., solar zenith angle (SZA), view zenith angle (VZA) and relative azimuth angle (RAZ). We perform one simulation for each of the 74 granules with clear sky pixels covering the South Pole. The mean solar zenith angle from all selected clear sky pixels from the same granule is input to the model as described in Section 2.1. The simulated reflectance representing individual pixel's VZA and RAZ are then averaged to represent mean model reflectance for the time and are compared with the mean reflectance from the collocated EPIC measurements. The simulation is set up in this way because the model runs one solar zenith angle at a time but outputs reflectance for different VZA and RAZ in a single simulation. Using the mean solar zenith angle minimizes the number of total simulations needed. Note that the RTM uses geometric definition at the top of atmosphere (TOA), 100 km above the sea level to be more precise. The EPIC geometric angles defined at the surface have to be converted to TOA for the input SZA and the computed reflectance angles (VZA and RAZ) have to be transferred back to the surface angles [27].

The following list is a summary of input and sensitivities for EPIC simulator:

- Clear sky selection requires both clear from ground observation and EPIC cloud mask
- Sounding is selected at ~12UTC; EPIC granule is selected within 0.25 hr of the sounding, and pixels less than 0.1° to 90°S
- Mean solar zenith angle (SZA) from EPIC pixels converted to TOA SZA
- Spectrally varying albedos from Antarctic snow surface observations
- Ground height (2.839 km)
- Vertical profiles of total, H₂O, O₂, CO₂, O₃ are modified based on observations
- Sensitivities for total O₃ and O₂ amount and presence of thin ice crystals
- Sensitivities with reduced surface albedo and BRDF versus Lambertian surface

2.3. Statistical tests

Both student-t-test and Mann-Kendall test are frequently used to determine the confidence of trends in time series of climate and hydrology data [e.g., 28,29]. The Mann-Kendall test is a non-parametric test that is suitable when there is missing data in time series, the distribution is non-normal, or the data set is censored. The null hypothesis is that there is no trend [30,31], while the hypothesis states that there is a monotonic trend over time. The method computes the net increasing or decreasing pairs of data points in a time series and a variance of this parameter based on the length of time series. The statistical confidence of the trend is computed by assuming the number of net pairs follow a normal distribution for randomly distributed time series. A larger number of net increasing or decreasing pairs would then find smaller

p-value in this distribution and higher confidence of a real trend.

Besides using a linear regression method to compute the trend, we also estimate the trend using Sen's slope [32], which seeks median slope of all data pairs in the time series. The Sen's slope is found to be less sensitive to skewness of data distribution or large outliers [33,34]. Mann-Kendall and Sen's slope are often computed together to estimate the slope and confidence of a trend. Details on Sen's slope estimator and the Mann-Kendall test are described in Yue and Pilon [35]. We applied student-t-test for quick trend estimate and Man-Kendall and Sen's slope for detailed trend analysis for both observed and simulated clear sky O₂ band ratios.

3. Results

3.1. Time series of 4 oxygen bands in EPIC observation

We start by collecting all collocated EPIC clear sky measurements within 0.1° of South Pole and 0.5 hof surface sky measurements in the months of December and January from December 2015 to January 2022, spanning 7 austral summers except for the period December 2019 to January 2020 when EPIC was in safe mode (27 June 2019 to 2 March 2020) and not collecting data. The clear sky pixels require both surface sky to be identified as clear (no cloud) and the EPIC cloud mask (which uses O₂ band ratios for cloud detection over snow surface) as clear [4]. To illustrate all data in a continuous time series, we mark days from December 1, 2015 to January 31, 2016 as Day 1 to 62, and December 1, 2016 as Day 63 and so on. Fig. 1 shows the four reflectance time series of B-band and A-band as well as the A-band and B-band ratios. The bidirectional reflectances (BRF) of the A-band and B-band reference channels are close to 0.99 and 0.97, respectively, and the absorption bands

have a value of about 0.27 and 0.54, respectively. The variations in reflectance are small albeit obvious, which is partially due to the randomly changing atmospheric conditions. Besides those random fluctuations, there is a visible seasonal cycle within each two-month period, which could be related to the procession of solar zenith angles. Most importantly, simple linear regressions indicate negative trends for both reference channels. The A-band and B-band absorption channels however display trends in the opposite direction. Although the slopes of these trends are small, they are statistically significant with larger than 99% confidence level based on the student-t-test except for the A-band absorption channel. Both ratios indicate a positive trend with over 99% confidence level. The question is whether changes in the observed atmospheric conditions and sun-sensor geometry are sufficient to explain the trends in the observed reflectance and ratios. Is there any residual trend or uncertainties that can't be unaccounted for which might be related with instrument calibration?

3.2. Model simulations

In order to understand the variability and trends in observed the EPIC reflectance over the south pole, we conducted RTM simulations with observed atmospheric vertical profiles wherever possible. Section 2.2 described the method of computing total H₂O, O₂, O₃ molecular density from radiosonde and ozonesonde and sets of spectral surface albedos we chose for the South Pole. Fig. 2 shows the time series of 74 simulated mean reflectance as compared to those observed. Only data from the first 4 years (December 1 to January 31, 2019) are shown in Fig. 2 because 1200Z sounding data in the last two winters are infrequent. Each point represents the average of at least 2 clear EPIC pixels viewing the South Pole for the given time. These pixels have

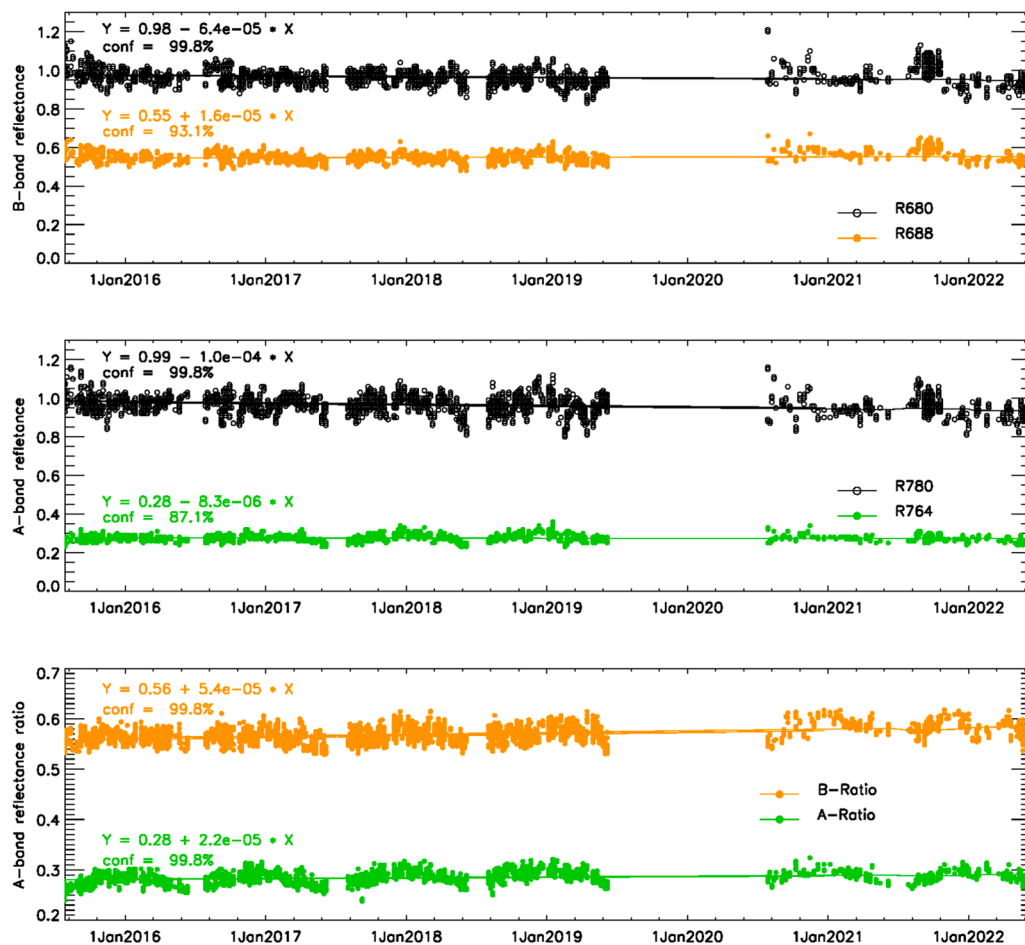


Fig. 1. EPIC O₂ A- and B-band observations over the Amundsen–Scott South Pole Station. Data are for the months of December and January from 2015 to 2022, except December 2019 and January 2020 when DSCOVR was off-line on the safe hold mode. Note that the time series was constructed as such that one Dec-Jan section is immediately followed by the next Dec-Jan section for trend computation, but a small gap is added in the plot between each data section to indicate there is a jump of time between one austral season to the next. Only clear sky observations are selected based on surface reports and the EPIC cloud mask. (a) BRF for the B-band absorption (R688, orange) and reference channels (R680, black); (b) BRF for the O₂ A-band absorption (R764, green) and reference channels (R780, black); and (c) channel ratios.

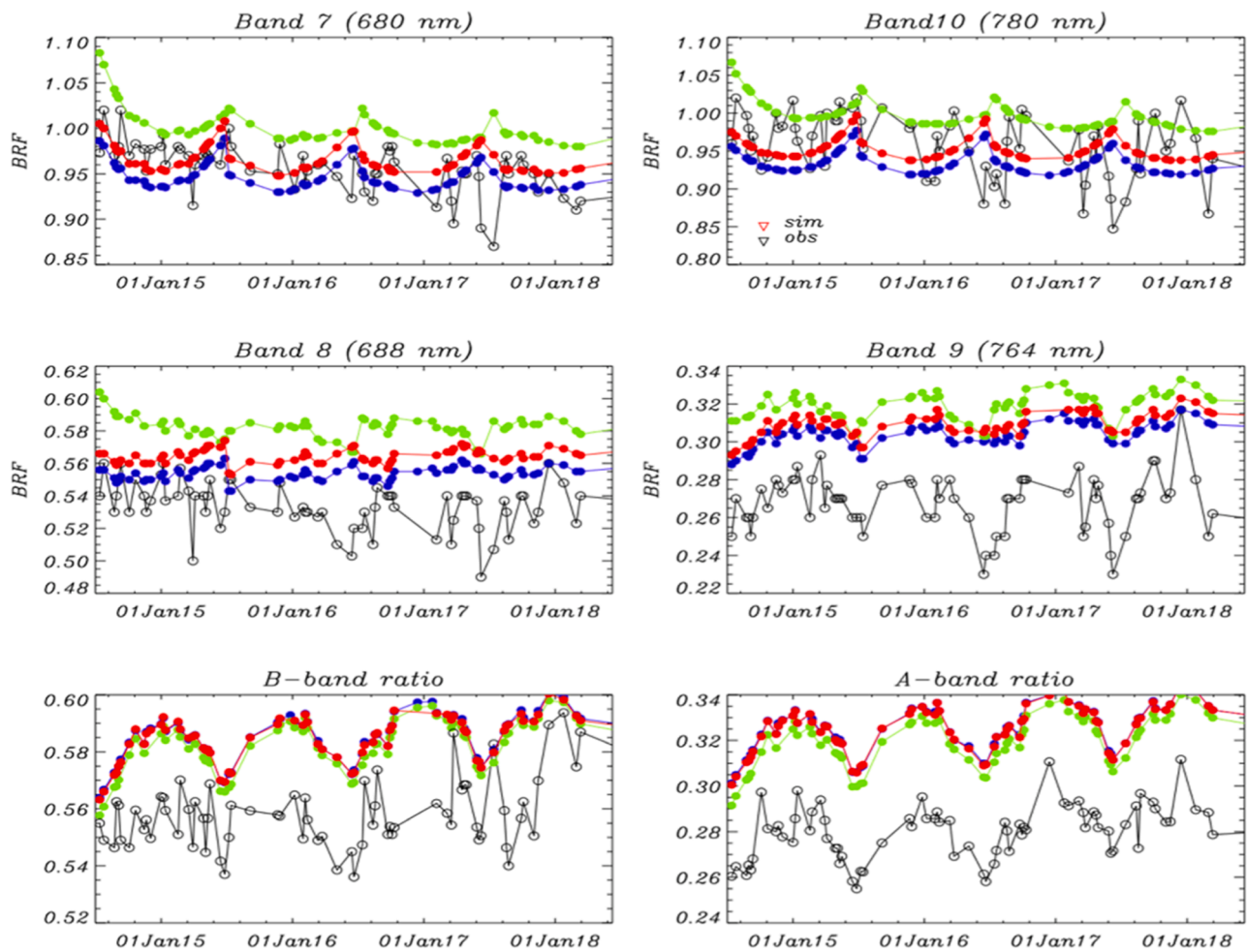


Fig. 2. The mean clear sky reflectance from the EPIC observations (black), model simulations with observed varying spectral albedo and snow surface BRDF (red), simulations with surface BRDF but reduced spectral albedo ($\text{alb} \cdot 0.98$) (blue), simulation with observed spectral albedo but Lambertian surface (green). The figure illustrates the difficulty of matching the simulated reflectance with observations even with the best estimates of spectral surface albedo and atmospheric profiles.

approximately the same SZA ($\sigma < 0.05$) and differences in viewing angles are taken explicitly into consideration.

In Fig. 2, the red dots represent the best effort simulations (BES) – the EPIC simulator was input with observed atmospheric sounding, column total ozone, and varying spectral albedos in addition to a snow surface BRDF based on Dome C observations [26] implemented particularly for this study. The measured spectral albedo for 680 nm, 688 nm, 764 nm and 780 nm bands are approximately 0.965, 0.96, 0.93, 0.92, respectively. Even though the observed reflectance in the non-absorbing 680 nm and 780 nm channels are quite noisy as compared to simulations, the overall matching for these two channels seems to be quite well, with a mean bias of 0.97% and -0.50% , and standard deviation of 3.06%, and 4.88%, respectively. The simulated reflectances in 688 nm and 764 nm bands follow the variability of observations better, but the magnitude is much higher than the observations, with a mean overestimation of 5.76% and 15.63% for 688 nm and 764 nm and standard deviation of 2.96% and 4.99%, respectively. The simulated B-band and A-band ratios are higher than those from observations by 4.74% and 16.09%, respectively. The high discrepancy between the observed and simulated O_2 band and ratios, especially at the A-band, suggests that major bias in the model input/simulation and/or instrument calibration could exist. Since the algorithm for retrieving EPIC cloud effective pressure (CEP) relies on lookup tables generated by the same model, it is our interest to understand the causes of these differences and determine whether an adjustment to LUT is necessary.

Matching model simulations with observations is an extremely tricky

problem [36,37]. The accuracy of model simulations is limited by the uncertainty of the inputs to the model, and model's inherent assumptions and simplifications. Ideally, such evaluation requires a complete set of surface and atmospheric measurements, such as surface albedo, atmospheric composition of all gasses used to drive the RTM. In reality, only radiosonde measurements of temperature, pressure and humidity and ozone measurements are available. Column ozone is interpolated from once every 5-day measurements. Snow albedo and surface BRDF is taken from a study in 2006 at Dome C (another Antarctic site) other than South Pole [26]. Not only the measurements of spectral albedo and BRDF could be associated with some uncertainty [26], the ground and snow condition at South Pole could also be slightly different from the that of Dome C site. It is anticipated both spectral albedo and surface BRDF could be a great source of uncertainty due to the large variability of surface snow anisotropy at high solar zenith angles. In terms of the RTM accuracy, the simulations at high solar and view zenith angles can be highly biased from a model with plane parallel assumptions. The current EPIC simulator has implemented an improved pseudospherical sphere (IPSS) approximation and its accuracy has been well validated on a black surface, but not on a high albedo surface, which remains an open task depending on the availability of benchmark data [22].

Another source of the discrepancy may originate from the instrument measurement uncertainty. While much of the instrument's uncertainty comes as random error, over the time the instrument needs continuous calibration to correct any possible deterioration. Because of the lack of in-flight absolute calibration of the O_2 absorption bands, EPIC's

measurements can't be considered as absolute "truth", which means that when we compare model results with observations, we can't treat either one as absolute "truth" and any discrepancy between model simulations and observations needs more careful evaluation.

In the following, we will discuss each of these factors, and conduct sensitivity studies when necessary.

3.2.1. Surface albedo and BRDF

Surface albedo or BRDF directly affect clear sky TOA reflectance, even more so at South Pole because the atmosphere is thin (surface pressure is only about two thirds of sea level pressure).

In general, the snow looks brighter when viewed near the horizon, in the forward direction, and darker when viewed near nadir, in the backward direction; and this anisotropy increases with increasing solar zenith angle and decreasing with surface albedo [26]. Anisotropic Factor (AF), which is calculated as bidirectional reflectance normalized by reflectance of an equivalent Lambertian surface of the same spectral albedo, is a measure of anisotropy in reflectance distribution at given solar zenith angle. According to the BRDF measurements at Dome C site, AF at 600 nm and 68° SZA in the backward direction (view zenith angle $\sim 67.5^\circ$ and azimuth angle $>160^\circ$ is between 1.0 and 1.3 [26]. At 680 nm and 780 nm, the backward AF could range from slightly below 1 to 1.2 within our angle range. The surface BRDF will not translate directly to TOA BRDF because of intervening atmosphere's scattering and absorbing effect. At visible shorter wavelength, the Rayleigh scattering will enhance the radiation in both forward and backward high solar and view zenith angle direction and reduce radiation in the direct beam direction. At NIR absorbing channels, the high amount of gaseous absorption at high zenith angles will reduce the radiation resulting in different BRDF patterns [38].

Even though we have implemented spectrally varying albedo and snow surface BRDF, the observation-based spectral albedo and BRDF from Dome C could be slightly different from South Pole. First, snow reflectivity changes with snow grain size, soot contamination and surface roughness and slope. It is reported that a kind of snow dune 'sas-trugi' often forms at high plateau of Antarctic in response to prevailing wind direction that could significantly affect snow reflectivity [25]. It is also likely that the ground is not completely flat and other non-snow objects such as station structure could be in field of view in a large satellite pixel. Therefore, it is difficult to get a complete realistic real-time surface spectral albedo and BRDF representing the entire domain of a large satellite pixel.

In order to understand the sensitivity of TOA reflectance to the uncertainties in spectral albedo and BRDF, we have run two sensitivity tests. The first sensitivity is run with a uniformly reduced albedo of 2% ($\text{alb} \cdot 0.98$) from the BES (blue dots), and a second sensitivity is run with the same spectral albedo as the BES but a Lambertian surface (green dots) (Fig. 2). The 2% reduction of spectral albedo results in an average decrease of reflectance in 680 nm, 780 nm, 688 nm, 764 nm bands by 1.93%, 1.96%, 1.89%, 1.85% respectively. It is worth noting that surface albedo has less effect on the absorption bands than the non-absorption bands.

Since the non-absorbing bands are matched well in the BES, there is no point to suggest that the spectral albedos in these two bands should be adjusted. To match the 688 nm and 764 nm bands with the observations, the albedos for these two bands have to drop from current 0.96 and 0.93 to around 0.90 and 0.78, respectively. This would be highly unlikely especially for the A-band since spectral snow albedo over Antarctic continent has 2~4% uncertainty [25].

While a snow BRDF does decrease the reflectance in the backward direction from Lambertian surface by 3.53%, 4.51%, 3.04% and 2.88% in 680 nm, 780 nm, 688 nm, 764 nm bands respectively, the empirical BRDF model uncertainty of 2~4% [26] plus site difference should not create any difference in reflectance larger than these numbers.

Unsurprisingly, a uniform percentage reduction or increase of spectral albedo will not lead to much change in the oxygen band ratios (less

than 0.11%), while the snow BRDF could slightly increase the A-band and B-band ratios by 1.70% and 0.50%, respectively, because it reduces the absorption bands less than the non-absorption bands in the backward direction. This makes neither spectral albedo nor BRDF a possible culprit for the large discrepancy between A-band and B-band ratios.

3.2.2. Meteorology

The second main factor comes from the uncertainty of meteorology (atmospheric profiles and molecular density) that are inputs to the model. The meteorology determines the total amount and vertical distribution of molecules that scatter and absorb lights. For the four channels this study focuses on, O_3 and O_2 are two major absorption gasses. The O_2 number density is estimated from total molecular density, which can be derived from radiosonde measurements of pressure and temperature. Typical radiosondes have reported errors of 1 °C for temperature and 2 mb for pressure and 5% relative humidity [39], which should transfer to less than 1.0% uncertainty in the total molecular density and subsequently O_2 molecular density. In addition, total O_2 amount in South Pole is quite stable with surface pressure varies between 674 mb to 697 mb from all the radiosonde measurements, and typically less than 6 mb or 1% of total amount from one day to the next. These factors suggest the uncertainty of input O_2 amount should be less than 2%.

On the contrary, total O_3 over South Pole has larger variability. The measured total ozone during the 7 austral summers ranges from 222 Dobson Unit (DU) to 454 DU, with measurements taken 5 days apart easily differ over 30 DU, which makes the interpolated total O_3 subject to large uncertainty. In addition, the ECC ozonesonde uncertainty could be more than 5% [40]. These factors contribute to an overall much larger uncertainty for the input total O_3 than the total O_2 . Besides the intrinsic instrument uncertainties mentioned above, the spatial temporal mismatch between satellite and sounding instruments means that the atmospheric volume covered within satellite field of view is not completely represented by the radiosonde or ozonesonde

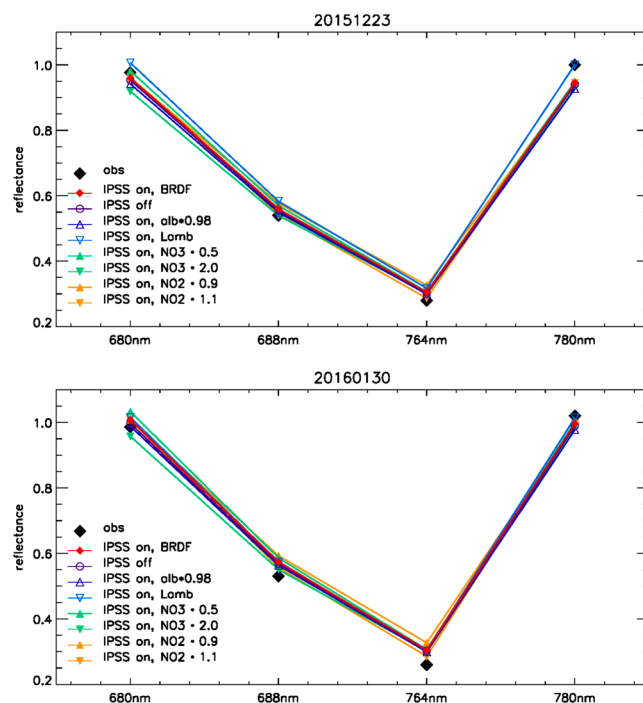


Fig. 3. Clear sky sensitivity tests with different surface albedo choices, column O_3 , O_2 , and model's spherical assumptions (IPSS on or off) on December 23, 2015 and January 30, 2016. Reflectance for four EPIC bands from various tests are shown in colored symbols, EPIC observed reflectance is shown in solid black circles.

measurements.

To account for the uncertainties of these atmospheric measurements, we conducted sensitivities on column O_3 and O_2 by multiplying the original O_3 profiles by 50% and 200%, and O_2 profiles by 90% and 110%, respectively, loosely based on their natural variability at South Pole, measurement frequency, and accuracy, etc., as discussed above, with possibly an order larger than their actual uncertainties.

Fig. 3 shows that the largest impact of O_3 occurs at 680 nm, however, its impact on A-band ratio and B-band ratio is minimal (Table 1). For the O_2 variation, the impact on the two absorbing bands, 688 nm and 764 nm, is the largest as expected. In fact, an artificial increase in O_2 amount by 10% will make the model simulated A-band and B-band ratios decrease by about 6.2% and 3.8% respectively, potentially filling approximately half of the simulation and measurement gaps (Table 1). However, as discussed above, the actual uncertainty of total O_2 amount should be no larger than 2% at South Pole, therefore its impact on 764 nm reflectance should be much smaller than 2% as well. Furthermore, these measurement errors are random, while the simulation indicates a more systematic overestimates of the reflectance in the absorption band.

To put these atmospheric profile sensitivities in perspective, we conducted a sensitivity by setting O_2 amount to zero in one of the profiles (without changing the amount of total molecular density hence molecular scattering). Table 2 lists the total absorption optical thickness from a reference simulation (Row 1), and profiles with zero O_2 (Row 2) and the difference between the two simulations (Row 3). It is clear that O_2 absorption is dominant at 688 nm and 764 nm, but other traces absorption is not zero, especially at 688 nm, which is about 1.5% of total absorption. At 764 nm, other trace absorption only contributes to 0.18%. While total absorption optical thickness for the two reference channels is small (0.0129 for 680 nm and 0.0026 for 780 nm) O_2 contribution is close to zero in these reference channels. This table explains why the uncertainties in the meteorological profiles, especially the O_3 has little impact on the reflectance. The column O_2 amount could greatly affect the absorption bands, but it has relatively low measurement uncertainty.

3.2.3. Background aerosol and diamond dust

A small amount of boundary layer aerosol and ice crystals could exist in the air even under clear sky conditions as diamond dust may occur over the South Pole. We tested such effect with a thin layer of ice cloud with optical thickness (COD) of 0.03, 0.1 and 0.3 in the boundary layer with cloud height (CHT) at 0.66 km and 1.66 km above ground.

Fig. 4 shows that thin clouds affect the TOA reflectance in a complex way. Generally the reflectances in all 4 bands decrease when thin ice cloud is present, the percentage change varies depending on optical thickness and time (geometry) of the pixel. The A-band and B-band ratios also decrease, but at a much smaller magnitude (Table 3). For a very thin cloud with optical thickness 0.03, the reflectances of all four channels decrease minimally around 1%. With optical thickness of 0.1, the R_{abs} decrease more than R_{ref} , resulting in small decreases in the O_2 band ratios, where B-band ratio decreasing slightly more than the A-band. When optical thickness reaches 0.3, even though the reflectance of

Table 1

Observed and computed A-band and B-band ratios with different clear sky input sensitivities in Fig. 3. The first row represents “best effort simulation” (BES) where the model has IPSS and BRDF on, and input with observed spectral albedos. Subsequent rows each have one condition modified from BES. For example, ‘ $\alpha \cdot 0.98$ ’ refers to simulations with 98% albedo (a 2% reduction) applied to all bands while the rest of the model input the same as BES.

Atmospheric Input/	680 nm	688 nm	764 nm	780 nm
Reference	0.012906	0.711949	1.36888	0.002611
Zero O_2 (Other trace gasses contribution)	0.012906	0.010768	0.002538	0.002611
Reference - Zero O_2 (O_2 contribution)	0.0	0.701180	1.36634	0.0

Table 2

Contributions of O_2 and other trace gasses to total absorption optical thickness at South Pole simulated with a reference sounding profile (23Dec, 2015). Row 1 and Row 2 are computed total absorption optical thickness with and without O_2 respectively.

Sensitivity case	B-band ratio	A-band ratio
IPSS on, BRDF	0.583	0.323
IPSS off, BRDF	0.582	0.322
IPSS on, BRDF, $\alpha \cdot 0.98$	0.583	0.323
IPSS on, Lambertian Srf	0.579	0.316
IPSS on, BRDF, $N_{O_3} \cdot 0.5$	0.580	0.323
IPSS on, BRDF, $N_{O_3} \cdot 2.0$	0.587	0.322
IPSS on, BRDF, $N_{O_2} \cdot 0.9$	0.601	0.345
IPSS on, BRDF, $N_{O_2} \cdot 1.1$	0.565	0.303
EPIC Observation	0.553	0.280

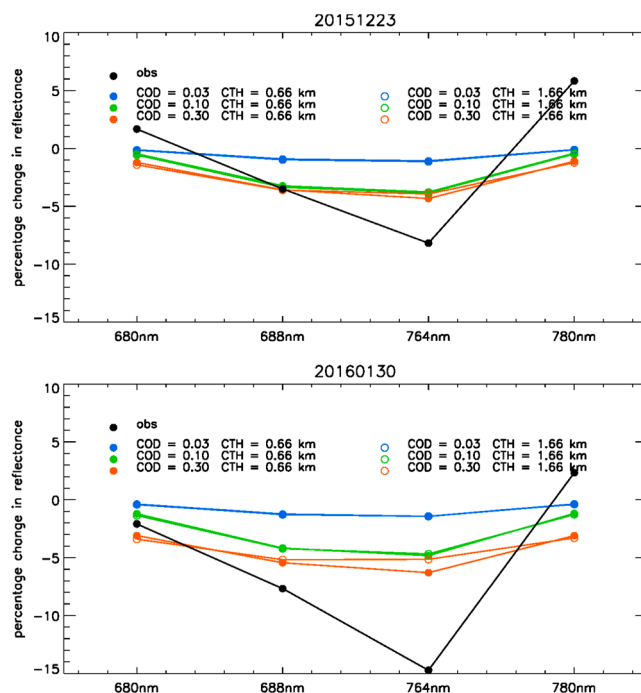


Fig. 4. Sensitivity tests with a thin layer of ice clouds with varying cloud optical Depth (COD) and cloud top height (CTH) for potential boundary layer ice (diamond dust) contamination on December 23, 2015 and January 30, 2016. Percentage changes of reflectance from simulation of clear sky with the same atmospheric profile are shown. The black dots indicate the percentage difference of EPIC observations from the same clear sky simulations.

Table 3

Changes in A-band and B-band ratios from that of clear sky from sensitivity tests of thin ice cloud in Fig. 4 on December 23, 2015.

Sensitivity tests / Change in ratio	Changes in B-band ratio	Changes in A-band ratio
COD = 0.03, CTH=0.66 km	-0.0046	-0.0031
COD = 0.10, CTH = 0.66 km	-0.0161	-0.0108
COD = 0.30, CTH = 0.66 km	-0.0139	-0.0105
COD = 0.03, CTH = 1.66 km	-0.0048	-0.0033
COD = 0.10, CTH = 1.66 km	-0.0163	-0.0110
COD = 0.30, CTH = 1.66 km	-0.0129	-0.0089

individual bands decreases more, the ratio decreases less than the 0.1 COT case. This shows a limitation of how much thin clouds can reduce the oxygen band ratios as most thick clouds tend to increase the ratios. This is consistent with sensitivities derived from previous studies [4], albeit the EPIC simulator in this study uses the new IPSS and BRDF

treatment. The maximum decrease in A-band and B-band ratios are 0.011 (3.6%) and 0.016 (2.8%), respectively, in these sensitivity tests, which are not sufficient to close the gap between the simulation and observations.

3.2.4. Earth's sphericity

Lastly, from the model's perspective, the EPIC simulator has been evaluated with and without the IPSS treatment. The Earth's spherical effect on light-scattering is increasingly more important as the sun and view zenith angles increase. To evaluate how IPSS assumption affects the TOA reflectance over South Pole, we run a sensitivity of the model with IPSS (IPSS on) and without IPSS (IPSS off) with the same surface spectral albedo and BRDF (Fig. 3). We notice that without proper treatment of the earth's sphericity, the RTM will generate slightly larger reflectance at non-absorbing bands while slightly decreased reflectance at strong absorbing band, but the net change (reduction) in ratio is less than 2% (Table 2).

3.2.5. Spectral response function

In the above analysis, we have explored all potential factors from model input perspective that could affect the EPIC simulations. None of the factors will affect the simulations for more than 2~3%. Aside from the amount of atmospheric oxygen that will exclusively affect the O₂ absorption bands, the surface albedo and diamond dust (thin ice clouds) should have similar impact for the absorption bands and the nearby non-absorption bands. However, the large differences are only seen in the O₂ absorption bands, which indicates that these input factors are unlikely to be responsible for the large biases in O₂ absorption bands. Here we will consider another aspect of the simulation that is not related to the input, but the instrument itself, i.e., the instrument response function (IRF). IRF determines spectral band width and shape and is convolved with RTM calculations to mimic what EPIC instrument will see. IRF is affected by all components of the instrument (e.g., filter, mirror, electronic recording system) and carefully measured as part of the pre-launch instrument calibration. IRF is subject to uncertainty and change over time, and instrument calibration is usually a continuous effort through the mission. The lack of onboard calibration and difficulty of cross-platform calibration for EPIC's oxygen bands have prompted use of lunar calibration for the oxygen bands [1,10,11]. However, the lunar calibration would not be able to capture small changes in the IRF of the oxygen bands since the light does not encounter any oxygen in the path.

To investigate potential inconsistency in our assumed pre-launch IRF in the EPIC simulator and the actual IRF, we conducted several experiments to examine whether small shifts of IRF in the absorption bands will create large difference in the simulated reflectance. We start by shifting the entire IRF by ± 0.1 nm, ± 0.2 nm, etc. and redo the clear sky simulations for all the clear sky samples. We find that by shifting the B-band (A-band) IRF by -0.2 nm (-0.3 nm), we can significantly reduce the percentage bias in 688 nm (764 nm) down to 0.51% (2.75%). Further shifting will increase the bias again (Table 4). This means the EPIC's O₂ bands are extremely sensitive to the center of bands and slight miss-characterization of IRF will create a large difference in the reported reflectance. Since EPIC's lunar calibration will not be able to detect such inaccuracy or shift in IRF, and we have ruled out other input factors, it is very likely the actual IRF has changed from pre-launch IRF.

Table 4

Mean percentage bias with small shift in IRF in EPIC simulator for all clear sky simulations in the months of December and January from 2015 to 2022.

Sensitivity tests	B-band bias	A-band bias
No shift	5.76%	15.62%
Shift -0.2 nm	0.51%	5.91%
Shift -0.3 nm	3.72%	2.75%
Shift -0.4 nm	10.49%	2.85%

3.3. Orbital change and reflectance trends

Fig. 2 illustrates the difficulty of matching the simulated reflectance with observations even with the best estimates of spectral surface albedo and atmospheric profiles. However, the shape of the variability within each two-month period and the overall trends are captured by the simulations. As expected, the sun-viewing geometry is consistently changing within the season (Fig. 5). While the SZA reaches the lowest point around December 23 each year, the lowest VZA lags behind the lowest SZA, and is progressively getting lower during this 7-year period due to the satellite orbital change. The RAZ has progressed from positive 10° to negative 10° as the satellite orbit changes. The scattering angle has reached 178° around December 2020 [41], positioning the sensor closer to complete backscattering direction.

In our previous study, we utilized the O₂ band ratios to detect clouds over snow and ice surfaces [4]. With single scattering approximation, we find that clear sky O₂ band ratios can be expressed as a function of total air mass and altitude. The total air mass, m , computed as summation of reverse cosine of SZA and VZA (Eq. (5)), represents total light path for the incoming and directly reflected sunlight. Larger SZA and VZA contribute to a larger total air mass and more oxygen absorption in the path and a smaller O₂ band ratio. On the other hand, higher altitude reduces the total path length and absorption, resulting in a larger O₂ band ratio.

The analytical derivation of the relations is as follows:

$$m = \frac{1}{\mu} + \frac{1}{\mu_0} = \frac{1}{\cos\theta} + \frac{1}{\cos\theta_0} \quad (5)$$

$$R_{\text{abs}} = T_{\text{abs}}^{\text{dn}} * \alpha_{\text{abs}} * T_{\text{abs}}^{\text{up}} = \alpha_{\text{abs}} e^{-(\tau(\rho(z)) + \tau_{\text{ray}}(\rho(z))) * m} \quad (6)$$

$$R_{\text{ref}} = T_{\text{ref}}^{\text{dn}} * \alpha_{\text{ref}} * T_{\text{ref}}^{\text{up}} = \alpha_{\text{ref}} e^{-\tau_{\text{ray}}(\rho(z)) * m} \quad (7)$$

$$\frac{R_{\text{abs}}}{R_{\text{ref}}} = \frac{\alpha_{\text{abs}}}{\alpha_{\text{ref}}} e^{-\tau(\rho(z)) * m} \quad (8)$$

where R_{abs} and R_{ref} are the BRF for the oxygen absorption and reference bands, respectively. BRF at the top of the atmosphere is a product of downward transmittance (T^{dn}), spectral surface reflection albedo α , and upward transmittance (T^{up}). τ and τ_{ray} are optical thickness values due to the O₂ absorption and Rayleigh scattering at nadir, respectively, and are functions of surface elevation and O₂ molecular density. In our previous study, we assumed albedos for the absorption and reference band are the same, and absorption optical thickness τ is only a function of surface height. This is a good approximation as surface altitude largely determines surface air pressure, hence total O₂ amount and absorption optical depth (Eq. (9)).

$$\tau(z) = K_a \rho_0 H \exp\left(-\frac{z}{H}\right) = c * \exp\left(-\frac{z}{H}\right) \quad (9)$$

$$\ln\left(\frac{R_{\text{abs}}}{R_{\text{ref}}}\right) = \ln\left(\frac{\alpha_{\text{abs}}}{\alpha_{\text{ref}}}\right) - \tau(\rho(z)) * m \quad (10)$$

$$\ln\left(\frac{R_{\text{abs}}}{R_{\text{ref}}}\right) = a + b * m \quad (11)$$

Here H is the scale height, and K_a, ρ_0 are the absorption coefficient, volume number density of oxygen, at sea level, respectively. $c = K_a w_1 \rho_0 H$, and was assumed constant in that study. In the current case, we maintain different albedos for the O₂ absorption and reference band, but the ratio of albedos remains constant. With surface altitude z being constant at one fixed location, and minimal variation in air density (pressure), optical thickness can be considered semi-constant. A more simplified relationship can be derived that shows the logarithm of the O₂ band ratio expressed as a linear function of air mass (Eq. (10)), which could be demonstrated as a linear regression form (Eq. (11)) in the actual model

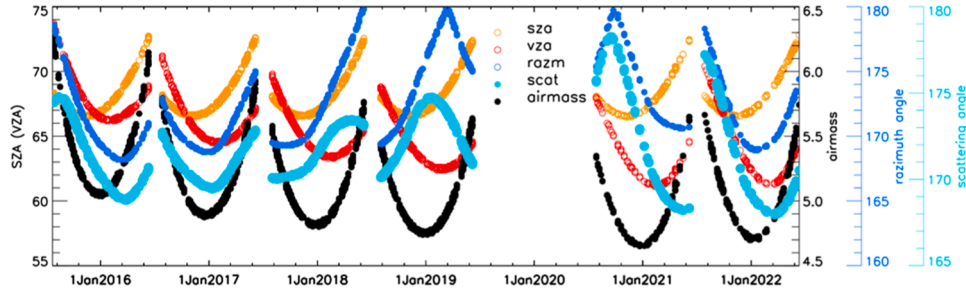


Fig. 5. Sun-viewing geometry of EPIC pixels over South pole during the past 7 austral summers. Note a small gap is added between each Dec-Jan time section as in Fig. 1.

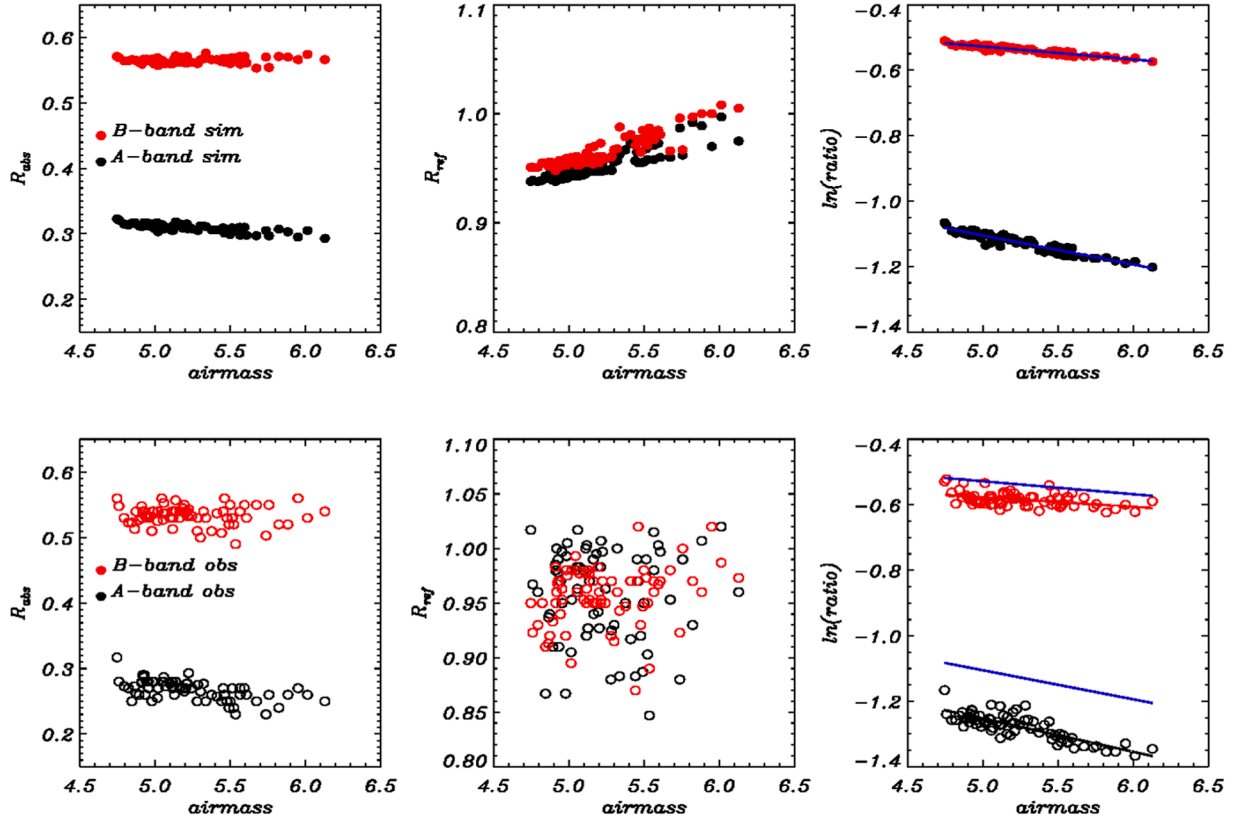


Fig. 6. (top) Model simulated O_2 band reflectances and ratios as a function of airmass. (bottom) Observed O_2 band reflectances and ratios as a function of airmass. The red and black dots represent the B-band and A-band reflectances or ratios, respectively. Blue lines indicate regression line from model simulated ratios in the left panel, while the black lines are regression line from the observed ratios.

simulation data as well as observed data.

Fig. 6 (top) shows the relationship of the O_2 band reflectances and ratios as a function of airmass. The absorption bands, especially the 764 nm, show better linear correlations with the airmass than the reference bands. The logarithmic of the O_2 ratio shows a good relationship as the single scattering theory predicted. The slight scatter of data points around the regression line is due to different atmospheric profiles that result in slightly different absorption optical thickness. The actual EPIC observations show similar relationship as the model simulations, with more scattering of data points due to measurement uncertainties (Fig 6, bottom). The regression lines from observations and simulations are nearly parallel in the final figure, but the offset differ, especially in the A-band, where the offset of observations (black line) is about 0.14 smaller than the simulations (blue line). We notice that a 15% smaller in observed A band ratio could translate into 0.1 smaller in the regression offset from Eq. (10). Of course, the same percentage difference in ratio of surface spectral albedos could have the same impact, but as we discussed

in Section 3.2.1, the albedo uncertainty is with 2~3%, and unlikely to cause such a large difference in offset.

On the other hand, because of this well-predicted relationship with airmass, it is reasonable to subtract this known physical dependence of the angles from the observations in order to analyze the observed “trend”. To do so, we compute the expected ratios from the regression fitting of the simulation data (Eq. (11)), and subtract them from the observed ratios (Eq. (12)). We then recompute the trends for the residual ratios to see if the trends remain significant.

$$\left(\frac{R_{abs}}{R_{ref}}\right)_{residual} = \left(\frac{R_{abs}}{R_{ref}}\right)_{obs} - \exp(a + b * m) \quad (12)$$

To be more rigorous regarding the confidence of the trends, we computed Sen’s median slope and the Mann-Kendall confidence for the trend. The Sen’s slope and Mann-Kendall analysis are non-parametric methods for assessing trend in a dataset and do not require the data to follow certain distributions (e.g. gaussian), therefore are more suited in

Table 5

Trends of A-band and B-band ratios from original EPIC observations, model simulations and the residuals.

	A_ratio_obs	A_ratio_sim	A_ratio_res	B_ratio_obs	B_ratio_sim	B_ratio_res
Student test (slope)	6.5e-05	6.2e-05	7.7e-06	5.7e-05	5.0e-05	1.3e-05
Confidence (%)	96.3	84.6	73.9	98.3	85.0	69.1
Sen's slope	6.2e-05	6.5e-05	5.6e-06	4.0e-05	5.1e-05	2.3e-08
Man-Kendall (%)	99.91	99.99	74.6	98.5	99.99	50.5

this problem. Table 5 shows that even though the student-t-test and non-parametric method do not always provide the same slope, they are quite close in magnitude for the observed A-band and B-band ratios. The slopes of model simulations are also similar in magnitude to the corresponding observations, which provides a justification for using the model's airmass relationship to subtract the angle dependence in the observational dataset since the model-based relationship has no instrument calibration issue. Furthermore, the time series of total absorption optical depth does not show significant trends, indicating that meteorology over the past 7 austral summers are not responsible for the trends in reflectance (Figure not shown). The angle corrected trend is an order smaller than the observations in A-band and less than half the magnitude in the B-band. The reason that the trend of B-band ratio is not reduced as significantly as the A-band ratio is due to less absorptive nature of the B-band, resulting in a weaker dependence of B-band ratio on the total airmass. In both cases, the Man-Kendall confidence for the ratios drop from 99% to below 90%. It is reasonable to conclude that with orbital change taken into consideration, both EPIC O₂ ratios do not show significant multiple-year trends. We thus conclude that the oxygen channels are reasonably stable over the past 7 austral summers.

4. Summary and discussion

The O₂ absorption bands in 688 nm and 764 nm play significant roles in the suite of DSCOVR EPIC's cloud products, including cloud mask, cloud effective pressure and other downstream products [3,41] and aerosol products [6,7,8]. Since EPIC was launched without an accurate laboratory calibration, and no instruments currently in space carry both narrow-band O₂ channels as EPIC does, the cross-platform calibration adopted by the EPIC science team to calibrate the UV and visible/NIR channels are not easily available for the 688 nm and 764 nm channels. The current indirect moon-view calibration has to use pre-assumed moon reflectance ratios and there is no built-in mechanism to detect IRF change from pre-launch to post-launch.

This study aims to evaluate the EPIC sensor stability with the EPIC measurements and radiative transfer simulations of O₂ bands over a uniquely suited location, i.e., the permanently snow-coverage South Pole. The EPIC simulator was developed with the pre-launch IRF and used to generate LUT for EPIC's cloud retrieval, therefore it is critical to make sure the model and instrument have the same response function. The study compares RTM simulations with in-situ measurements of atmospheric soundings from the Amundsen-Scott South Pole meteorological station with EPIC measurements taken during months of December and January from 2015 to 2022. We find that even in the clear sky measurements taken at around the same time of the year, small fluctuations within each two-month period, and small, but significant trends in the ratios of A-band and B-band are observed. The absolute discrepancy from the best RTM estimates and those of observations is about -0.50~0.97% for the two reference bands, but 5.76% and 15.63% for the 688 nm, and 764 nm absorption bands, respectively. Various input sensitivities are conducted including atmospheric profiles, column ozone, and surface spectral albedo and BRDF. The simulation results are sensitive to surface spectral albedo, BRDF, total oxygen amount, and cloud contamination, each of these could contribute to a maximum 2~3% bias in simulated reflectance based on our estimation, which sums to a total of 4~6% uncertainty of the absorption band reflectance and ratios if measurement errors are random. It is possible the spectral albedo and BRDF bias could be systematic, but this is

beyond the scope of this study.

Even though inputs to the model simulation are unlikely to account for the large biases in the oxygen band simulations, we find the simulations to be very sensitive to small shifts in the IRFs due to the narrow band width and sharp absorption lines of the oxygen bands. With a -0.2 nm and -0.3 nm shift of IRF, we are able to narrow the bias to 0.51% and 2.75% for the 688 nm and 764 nm bands, respectively. This indicates IRF could be the major factor responsible for the large bias in the simulations.

With regard to the more systematic variations and multi-year trends of the O₂ band ratios, the RTM simulations are able to capture this with realistic input of sun-sensor geometry angles. In fact, the O₂ band ratio variation can be predicted quite well by the total airmass, especially in the strong-absorbing A-band. We find the small orbital change of the satellite over the past seven years and the corresponding changes of geometric angles over South Pole is responsible for the observed trends in the O₂ band ratios. When model simulated contributions from the angle variations are deducted from the observed O₂ band ratios, the residual O₂ band ratios are found to be stable since 2015. Therefore, we are able to report with confidence that the oxygen channels are reasonably stable over the past 7 years consistent with other studies [42, 43]. It is suggested that the Lagrange 1 orbit provides a consistent space environment for the EPIC instrument and contributes to its stability as the instrument does not have to undergo periodic variations of extremely hot and cold temperatures like satellites in low Earth orbits which periodically move from sun to shadow every ~50 min [42]. In addition, the instrument is situated in a constant radiation environment as it is always facing the earth with the sunside properly shielded from damages of solar winds. Furthermore, the EPIC sensor only takes ~15 images a day, requiring only a second of exposure time a day with the rest of the time the shutters closed so that the instrument is less prone to degrading even in space environment.

However, it is still possible that the instrument had gone through some changes during its launch or the pre-launch calibration was not perfect, either condition would have made the true IRF different from what we use in the radiative transfer simulation. Through careful examination of all potential factors in the RTM simulations, we found that a small shift of the oxygen A and B band IRF can reduce the model and measurement discrepancy significantly. While further research is needed to figure out the exact combination of spectral shift and shape to represent the actual IRF, this study provides a pathway and justification to create new LUTs that match the actual observations. This will help improve other Level 2 cloud and aerosol retrievals. For example, in the CEP algorithm, insufficient absorption in the current LUT is consistent with the overestimation of CEP (retrieved cloud lower than the actual clouds to compensate) in the majority of the retrievals [3].

Declaration of Competing Interest

The authors declare the following financial interests/personal relationships which may be considered as potential competing interests:

Yaping Zhou reports financial support was provided by NASA. Pengwang Zhai reports financial support was provided by NASA.

Data availability

Data will be made available on request.

Acknowledgement

The authors thank Drs Alexander Marshak, Alexi Lyapustin, Xiaoguang Xu, Omar Torres for helpful discussions and two anonymous reviewers for their constructive comments. The work was supported through grants by the NASA DSCOVR program managed by R. S. Eckman. The authors appreciate the support of the University of Wisconsin-Madison and Madison College AMRDC for the South Pole data set, data display, and information, NSF grant number 1951720 (UW) and 1951603 (MATC). The Ozonesonde data is obtained from NOAA global monitoring laboratory.

References

- Marshak A, Herman J, Szabo A, Blank K, Cede A, Carn S, Geogdzhayev I, Huang D, Huang LK, Knyazikhin Y, Kowalewski M, Krotkov N, Lyapustin A, McPeters R, Meyer K, Torres O, Yang Y. Earth observations from DSCOVR/EPIC instrument. *Bull Amer Meteor Soc (BAMS)* 2018;9:1829–50. <https://doi.org/10.1175/BAMS-D-17-0223.1>.
- Marshak A, Lyapustin A, Schuster GL, Szabo A, Eckman R. Editorial: DSCOVR EPIC/NISTAR: 5 years of observing earth from the first lagrangian point. *Front Remote Sens Sec Satel Missions* 2022;3. <https://doi.org/10.3389/frsen.2022.963660>. 2022.
- Yang Y, Meyer K, Wind G, Zhou Y, Marshak A, Platnick S, Min Q, Davis AB, Joiner J, Vasilkov A, Duda D, Su W. Cloud products from the earth polychromatic imaging camera (EPIC) observations: algorithm description and initial evaluation. *Atmos Meas Tech* 2019;12:2019–31. <https://doi.org/10.5194/amt-12-2019-2019> [1].
- Zhou Y, Yang Y, Gao M, Zhai PW. Cloud detection over snow and ice with oxygen A- and B-band observations from the earth polychromatic imaging camera (EPIC). *Atmos Meas Tech* 2020. <https://doi.org/10.5194/amt-13-1575-2020>.
- Zhou Y, Yang Y, Zhai P, Gao M. Cloud detection over sunglint regions with observations from the Earth Polychromatic Imaging Camera (EPIC). *Front Remote Sens* 2021;2. <https://doi.org/10.3389/frsen.2021.690010>.
- Xu X, Wang J, Wang Y, Zeng J, Torres O, Yang Y, Marshak A, Reid J, Miller S. Passive remote sensing of altitude and optical depth of dust plumes using the oxygen A and B bands: first results from EPIC/DSCOVR at Lagrange-1 point. *Geophys Res Lett* 2017;44:7544–54. <https://doi.org/10.1002/2017GL073939>.
- Xu X, Wang J, Wang Y, Zeng J, Torres O, Reid J, Miller S, Martins JV, Remer L. Detecting layer height of smoke aerosols over vegetated land and water surfaces via oxygen absorption bands: hourly results from EPIC/DSCOVR in deep space. *Atmos Meas Tech* 2019;12:3269–88. <https://doi.org/10.5194/amt-12-3269-2019>.
- Lyapustin A, Go S, Korokin S, Wang Y, Torres O, Jethva H, Marshak A. Retrievals of aerosol optical depth and spectral absorption from DSCOVR EPIC. *Front Remote Sens* 2021;2. <https://doi.org/10.3389/frsen.2021.645794>.
- Herman J, Huang L, McPeters R, Ziemke J, Cede A, Blank K. Synoptic ozone, cloud reflectivity, and erythemal irradiance from sunrise to sunset for the Whole earth as viewed by the DSCOVR spacecraft from the earth-sun lagrange 1 Orbit. *Atmos Meas Tech* 2018;11:177–94. <https://doi.org/10.5194/amt-11-177-2018>.
- Geogdzhayev IV, Marshak A. Calibration of the DSCOVR EPIC Visible and NIR Channels using MODIS terra and aqua data and EPIC lunar observations. *Atmos Meas Tech* 2018;11:359–68. <https://doi.org/10.5194/amt-11-359-2018>.
- Geogdzhayev IV, Marshak A, Alexandrov M. Calibration of the DSCOVR EPIC visible and NIR channels using multiple LEO radiometers. *Front Remote Sens* 2021;2. <https://doi.org/10.3389/frsen.2021.671933>.
- Ohtake M, Pieters CM, Isaacson P, Besse S, Yokota Y, Matsunaga T, Boardman J, Yamamoto S, Haruyama S, Staid M, Mall U, Green RO. One moon, many measurements 3: spectral reflectance. *Icarus* 2013;226:364–74.
- Dubuisson P, Borde R, Dessailly D, Santer R. In-flight spectral calibration of the oxygen A-band channel of MERIS. *Int J Remote Sens* 2003;24(5):1177–82. <https://doi.org/10.1080/0143116021000031809>.
- Hagolle O, Goloub P, Deschamps PY, Cosnefroy H, Briottet X, Bailleul T, Nicolas JM, Parok F, Lafrance B, Herman M. Results of POLDER in-flight calibration. *IEEE Trans Geosci Remote Sens* 1999;37:1550–66.
- Lazzara MA, Weidner GA, Keller LM, Thom JE, Cassano JJ. Antarctic automatic weather station program: 30 years of polar observations. *Bull Amer Meteor Soc* 2012;93:1519–37. <https://doi.org/10.1175/BAMS-D-11-00015.1>.
- Sterling CW, Johnson BJ, Oltmans SJ, Smit HJ, Jordan AF, Cullis PD, et al. Homogenizing and estimating the uncertainty in NOAA's long-term vertical ozone profile records measured with the electrochemical concentration cell ozonesonde. *Atmos Meas Tech* 2018;11:3661–87. <https://doi.org/10.5194/amt-11-3661-2018>.
- Gao M, Zhai PW, Yang Y, Hu Y. Cloud remote sensing with EPIC/DSCOVR observations: a sensitivity study with radiative transfer simulations. *J Quant Spectrosc and Radiat Transf* 2019;230:56–60. <https://doi.org/10.1016/j.jqsrt.2019.03.022>.
- Zhai P, Hu Y, Trepte CR, Lucker PL. A vector radiative transfer model for coupled atmosphere and ocean systems based on successive order of scattering method. *Opt Express* 2009;17:2057–79. <https://doi.org/10.1364/OE.17.002057>.
- Zhai P, Hu Y, Chowdhary J, Trepte CR, Lucker PL, Josset DB. A vector radiative transfer model for coupled atmosphere and ocean systems with a rough interface. *J Quant Spectrosc Radiat Transf* 2010;111:1025–40. <https://doi.org/10.1016/j.jqsrt.2009.12.005>.
- Rothman L, Gordon I, Babikov Y, Barbe A, Benner DC, Bernath P, Birk M, Bizzocchi L, Boudon V, Brown LR, Campargue A, Chance K, Cohen EA, Coudert LH, Devi VM, Drouin BJ, Fayt A, Flaud JM, Gamache RR, Harrison JJ, Hartmann JM, Hill C, Hodges JT, Jacquemart D, Jolly A, Lamouroux J, Le Roy RJ, Li G, Long DA, Lyulin OM, Mackie CJ, Massie ST, Mikhailenko S, Müller HSP, Naumenko OV, Nikitin AV, Orphal J, Perevalov V, Perrin A, Polovtseva ER, Richard C, Smith MAH, Starikova E, Sung K, Tashkun S, Tennyson J, Toon GC, Yttrerev VIG, Wagner G. The hitran2012 molecular spectroscopic database. *J Quant Spectrosc Radiat Transf* 2013;130:4–50. <https://doi.org/10.1016/j.jqsrt.2013.07.002>.
- Buehler SA, Eriksson P, Lemke O. Absorption lookup tables in the radiative transfer model ARTS. *J Quant Spectrosc Radiat Transf* 2011;112(10):1559–67. <https://doi.org/10.1016/j.jqsrt.2011.03.008>.
- Zhai PW, Hu Y. An improved pseudo spherical shell algorithm for vector radiative transfer. *J Quant Spectrosc Radiat Transf* 2022;282. <https://doi.org/10.1016/j.jqsrt.2022.108132>.
- Caudill TR, Flittner DE, Herman BM, Torres O, McPeters RD. Evaluation of the pseudo-spherical approximation for backscattered ultraviolet radiances and ozone retrieval. *J Geophys Res* 1997;102(D3):3881–90. <https://doi.org/10.1029/96JD03266>.
- Barker HW, Stephens GL, Partain PT, Bergman JW, Bonnel B, Campana K, Clothiaux EE, Clough S, Cusak S, Delamere J, Edwards J, Evans KF, Fouquart Y, Freidenreich S, Galin V, Hou Y, Kato S, Li J, Mlawer E, Morcrette JJ, O'Hirok W, Raisanen P, Ramaswamy V, Ritter B, Rozanov E, Schlesinger M, Shibata K, Sporyshev P, Sun Z, Wendisch M, Wood N, Yang F. Assessing 1D atmospheric solar radiative transfer models: interpretation and handling of unresolved clouds. *J Clim* 2003;16:2676–99.
- Grenfell TC, Warren SG, Mullen PC. Reflection of solar radiation by the Antarctic snow surface at ultraviolet, visible, and near-infrared wavelengths. *J Geophys Res* 1994;99(D9). 18,669–18,684.
- Hudson SR, Warren SG, Brandt RE, Grenfell TC, Six D. Spectral bidirectional reflectance of Antarctic snow: measurements and parameterization. *J Geophys Res* 2006;111:D18106. <https://doi.org/10.1029/2006JD007290>.
- Korkin S, Yang ES, Spurr R, et al. Revised and extended benchmark results for Rayleigh scattering of sunlight in spherical atmospheres. *J Quant Spectrosc Radiat Transf* 2020;254:107181. <https://doi.org/10.1016/j.jqsrt.2020.107181>.
- Wilks DS. *Statistical methods in the atmospheric sciences*. 3rd ed. Oxford: Academic Press; 2011. ISBN: 9780123850225.
- Yue S, Pilon P, Cavadias G. Power of the Mann-Kendall and Spearman's rho tests for detecting monotonic trends in hydrological series. *J Hydrol* 2002;259:254–71. [https://doi.org/10.1016/S0022-1694\(01\)00594-7](https://doi.org/10.1016/S0022-1694(01)00594-7).
- Mann HB. Non-parametric tests against trend. *Econometrica* 1945;13:163–71.
- Kendall MG. *Rank correlation methods*. 4th ed. London: Charles Griffin; 1975.
- Sen PK. Estimates of the regression coefficient based on Kendall's tau. *J Am Stat Assoc* 1968;63:1379–89.
- Fernandes R, Leblanc SG. Parametric (modified least squares) and non-parametric (Theil-Sen) linear regressions for predicting biophysical parameters in the presence of measurement errors. *Remote Sens Environ* 2005;95(3):303–16. <https://doi.org/10.1016/j.rse.2005.01.005>. Bibcode:2005RSEnv..95..303F.
- Hirsch RM, Slack JR, Smith RA. Techniques of trend analysis for monthly water quality data. *Water Resour Res* 1982;18(1):107–21. <https://doi.org/10.1029/WR018i001p0107>.
- Yue S, Pilon P. A comparison of the power of the t-test, Mann-Kendall and bootstrap tests for trend detection / Une comparaison de la puissance des tests t de Student, de Mann-Kendall et du bootstrap pour la détection de tendance. *Hydro Sci J* 2004;49:21–37. <https://doi.org/10.1623/hysj.49.1.21.53996>. 1.
- Zhou YP, Cess RD. Validation of longwave atmospheric radiation models using Atmospheric Radiation Measurement data. *J Geophys Res* 2000;105(D24):29703–16. <https://doi.org/10.1029/2000JD900557>.
- Aumann HH, Chen X, Fishbein E, Geer A, Havemann S, Huang X, et al. Evaluation of radiative transfer models with clouds. *J Geophys Res Atmos* 2018;123:6142–57. <https://doi.org/10.1029/2017JD028063>.
- Zhou Y, Rutledge K, Charlock T, Leob N, Kato S. Atmospheric corrections using MODTRAN for TOA and surface BRDF characteristics from high resolution spectroradiometric/angular measurements from a helicopter platform. *Adv Atmos Sci* 2001;18(5):984–1004. <https://doi.org/10.1007/s00376-001-0018-0>.
- Lenhard RW. A revised assessment of radiosonde accuracy. *Bull Amer Meteorol Soc* 1973;54(7):691–3. <http://www.jstor.org/stable/26254246>.
- Tarasick DW, Smit HJ, Thompson AM, Morris GA, Witte JC, Davies J, et al. Improving ECC ozonesonde data quality: assessment of current methods and outstanding issues. *Earth Space Sci* 2021;8:e2019EA000914. <https://doi.org/10.1029/2019EA000914>.
- Marshak A, Delgado-Bonal A, Knyazikhin Y. Effect of scattering angle on earth reflectance. *Front Remote Sens, Sec Satel Missions* 2021;2. <https://doi.org/10.3389/frsen.2021.719610>. 2021.
- Cede A, Kang Huang L, McCauley G, Herman J, Blank K, Kowalewski M, Marshak A. Raw EPIC data calibration. *Front Remote Sens* 2021;2:702275. <https://doi.org/10.3389/frsen.2021.702275>.
- Haney C, Doelling DR, Su W, Bhatt R, Gopalan A, Scarino B. Radiometric stability assessment of the DSCOVR EPIC visible bands using MODIS, VIIRS, and invariant targets as independent references. *Front Remote Sens* 2022. <https://doi.org/10.3389/frsen.2021.765913>. 24 Front Remote Sens., 24 JanuarySec. Satellite Missions.